Earth Syst. Sci. Data Discuss., 8, 649–702, 2015
www.earth-syst-sci-data-discuss.net/8/649/2015/
doi:10.5194/essdd-8-649-2015

Open Access Earth System Science Data Discussions

High-resolution daily gridded datasets of air temperature and wind speed for Europe

S. Brinckmann[1], S. Krähenmann[2], and P. Bissolli[1]

[1]Climate Monitoring, Deutscher Wetterdienst, Frankfurter Strasse 135, 63067 Offenbach, Germany
[2]Central Climate Office, Deutscher Wetterdienst, Frankfurter Strasse 135, 63067 Offenbach, Germany

Received: 30 June 2015 – Accepted: 8 July 2015 – Published: 12 August 2015

Correspondence to: S. Brinckmann (sven.brinckmann@web.de)

Published by Copernicus Publications.

Abstract

New high-resolution datasets for near surface daily air temperature (minimum, maximum and mean) and daily mean wind speed for Europe (the CORDEX domain) are provided for the period 2001–2010 for the purpose of regional model validation in the framework of DecReg, a sub-project of the German MiKlip project, which aims to develop decadal climate predictions. The main input data sources are hourly SYNOP observations, partly supplemented by station data from the ECA&D dataset (http://www.ecad.eu). These data are quality tested to eliminate erroneous data and various kinds of inhomogeneities. Grids in a resolution of 0.044° (5 km) are derived by spatial interpolation of these station data into the CORDEX area. For temperature interpolation a modified version of a regression kriging method developed by Krähenmann et al. (2011) is used. At first, predictor fields of altitude, continentality and zonal mean temperature are chosen for a regression applied to monthly station data. The residuals of the monthly regression and the deviations of the daily data from the monthly averages are interpolated using simple kriging in a second and third step. For wind speed a new method based on the concept used for temperature was developed, involving predictor fields of exposure, roughness length, coastal distance and ERA Interim reanalysis wind speed at 850 hPa. Interpolation uncertainty is estimated by means of the kriging variance and regression uncertainties. Furthermore, to assess the quality of the final daily grid data, cross validation is performed. Explained variance ranges from 70 to 90 % for monthly temperature and from 50 to 60 % for monthly wind speed. The resulting RMSE for the final daily grid data amounts to 1–2 °C and 1–1.5 m s^{-1} (depending on season and parameter) for daily temperature parameters and daily mean wind speed, respectively. The datasets presented in this article are published at http://dx.doi.org/10.5676/DWD_CDC/DECREG0110v1.

ESSDD

8, 649–702, 2015

1 Introduction

In climate research data of meteorological observations are preferably provided in the form of continuous regular grids. In this way the data can be used for regional or global climate monitoring as well as for a comparison with the outputs from numerical weather prediction models and climate models. One of the main and most reliable initial data sources are measurements taken at ground station networks like SYNOP (synoptical observations recommended by the World Meteorological Organization (WMO)). Interpolation or averaging procedures are used to transform such point data to values representative for grid cells of regular size and distance.

For the near-surface temperature a variety of gridded observational data are available. One of the most prominent global datasets is the HadCRUT4 dataset provided by the UK Met Office Hadley Centre and the Climatic Research Unit (CRU) at the University of East Anglia (Morice et al., 2012), covering monthly values in 5° spatial resolution since 1850. In recent years several more global temperature datasets have been published (e.g., Smith et al., 2008; Hansen et al., 2010; Rohde et al., 2013). On a regional scale temperature datasets with higher resolutions in space (e.g. Hogewind and Bissolli, 2011) and time have been produced. For Europe the E-OBS project has set up an archive of gridded daily data in a horizontal resolution of 0.25° starting in 1950 (Haylock et al., 2008). Since regional models increasingly realize even higher resolutions, reference datasets with resolutions below 0.25° are more and more requested. So far, such data are only produced on a national or sub-regional scale.

In addition to the pure observational datasets so-called reanalysis data represent alternative sources. Measurements from surface stations, radiosondes and satellite data of different meteorological parameters serve as input data for the assimilation scheme of weather prediction models. 3-D gridded data for a variety of parameters describing the initial status of the atmosphere are obtained. However, the dependency on model physics make reanalysis data unsuitable for the evaluation of model forecasts.

ESSDD
8, 649–702, 2015

Concerning the near-surface wind speed, the availability of gridded observational data is currently very low. On a national level a few efforts have been made to calculate horizontal wind fields based on station reports (e.g., Luo et al., 2008; Gerth and Christoffer, 1994; Walter et al., 2006). For larger regions like Europe at present no such data fields are available.

Within DecReg (Decadal Regional Predictability), a subproject of MiKlip (Decadal Climate Predictions), the predictive skill of regional climate models on a decadal time scale is investigated using hindcast experiments. Independent gridded observational datasets for the European region are used as reference. In order to meet the spatial scale of these models (7 km for the COSMO-CLM model; http://www.clm-community.eu/), new reference data with resolutions below the 25 km realized by E-OBS are required. This request represents a big challenge, as the grid size is limited by the density of station observations. More complex interpolation methods are needed to maintain a certain quality on a relatively fine grid. As contribution to DecReg, the Deutscher Wetterdienst (DWD) aims to provide gridded observational data of daily temperature and wind speed in high resolution for the time period 1961–2010.

A variety of interpolation methods can be used to derive continuous field data based on point measurements (see overview given by e.g. Li and Heap, 2008). In cases of relatively coarse grid sizes (with a high number of samples per grid cell) simple averaging techniques are sufficient. For relatively fine grids the value at a given point has to be estimated on the basis of information of surrounding data points. Deterministic interpolation methods are based on the assumption of a certain function, which describes the spatial changes of the target variable. For example, linear regression on the coordinates x and y using least square fitting represents a simple form of a deterministic interpolator. A very prominent deterministic approach is the inverse distance weighting method (IDW), in which the information of nearby stations is used to determine the value at certain target coordinates, expecting a decrease of influence with increasing distance. An interpolation method involving probabilistic elements (often called a stochastic or geostatistic approach) is the so-called kriging (after Daniel G. Krige,

ESSDD
8, 649–702, 2015

further developed by Matheron, 1963). Compared to IDW in kriging the geographic distribution of the surrounding data points is considered (solving the cluster problem) and the weights are optimized by considering the spatial correlation observed for the target variable. In contrast to deterministic methods kriging directly provides uncertainty estimates for each grid point. Many meteorological parameters depend on certain local characteristics (like temperature and pressure on the altitude or wind speed on the surrounding vegetation and topography). Such secondary information can be included in the interpolation procedure by a regression approach.

In this work a combination of regression and kriging is used to compute gridded data in 5 km horizontal resolution of daily mean 10 m scalar wind speed and daily 2 m air temperatures (minimum, maximum and mean). Here, the results for the decade 2001–2010 are presented. Earlier decades are planned to be added to this new data record in the future.

2 Input data

The main input data source used in this work are SYNOP reports. Daily minimum temperatures (T_{min}, between 18:00 and 06:00 UTC) and daily maximum temperatures (T_{max}, 06:00 to 18:00 UTC) are directly available from the database at the DWD, while daily mean temperatures as well as daily mean wind speed, T_{avg} and V_{avg}, are derived from hourly reports (using data from 00:00 to 00:00 UTC of the following day). The European Climate Assessment & Dataset project (ECA&D, Klein Tank et al., 2002) offers additional station measurements for Europe and North Africa (data and metadata available at http://www.ecad.eu). 62 participating countries have provided quality-checked data records for numerous weather stations. For temperature the ECA&D record is used to extend the input data in areas with low coverage by SYNOP stations. Due to the issue of partly deviating daily reference periods for the three parameters (see discussion in Sect. 2.2) we apply a selection algorithm for the inclusion of ECA&D data. In this way we aim to avoid inconsistencies with the input data based on SYNOP. The accuracy of the meteorological data from both archives is limited by the precision of the reports (i.e., number of decimal places), which typically depends on the underlying measurement accuracy. Thus, basic uncertainties of 0.1 °C and approx. $0.5\,\mathrm{m\,s^{-1}}$ (1 knot) can be assumed for the two parameters.

2.1 Hourly SYNOP reports

Figure 1a shows the distribution of SYNOP stations reporting at least every 6 h (see color code for different frequencies) throughout the target domain for January 2010. In total 2230 stations are found. Most of the regions in the target domain (indicated by the red frame) are well covered, only for Africa larger regions without data are identified.

Daily T_{avg} and V_{avg} are derived by averaging the available hourly data, while assigning only half of the regular weight to the measurements at 00:00 UTC (of current and following day). To evaluate the consistency between daily means based on different sample sizes, these values were compared at stations with full daily records of 25 samples. In Fig. 2 the results for daily means in January 2001 based on 3 hourly and 6 hourly reports are displayed for temperature (panels a1, a2) and wind speed (b1, b2) respectively. For temperature we find a high consistency even for the 6 hourly reports (a2), with a standard deviation of the error of 0.21 °C. For wind speed the precision in the determination of the daily mean decreases considerably with the number of samples per day ($\sigma = 0.40\,\mathrm{m\,s^{-1}}$ for 6 hourly reports). But compared to the relatively high basic uncertainty of $0.5\,\mathrm{m\,s^{-1}}$ for wind speed data, these potential discrepancies are found acceptable. For 1 hourly reports up to two missing or non-valid data in a daily record of 25 values were accepted. In the calculation of the daily means these gaps were filled by the mean of the two adjacent dates. Daily records with report frequencies below one hour were rejected when missing values or inhomogeneities (see Sect. 2.3) occurred.

ESSDD
8, 649–702, 2015

2.2 Integration of ECA&D archive for temperature

The national weather services contributing data to ECA&D determined daily temperature parameters based on partly different reference intervals. For example, in some countries daily mean temperatures are based on the interval between 00:00 to 00:00 UTC, in other countries between 06:00 UTC and 06:00 UTC (van den Besselaar et al., 2012). Our experiments with station data at identical coordinates revealed consistency problems between SYNOP and ECA&D for all three parameters. Especially for winter days the discrepancy is ocasionally greater than 2 °C. Therefore, an algorithm was designed to carefully include data from the ECA&D archive, considering the density of SYNOP reports in each target area and by data comparison at identical stations (only if coordinates and station height agree for both archives). The differences at identical stations were used as indicator for the consistency in the target region for each day. Depending on the presence of SYNOP data in a certain area the thresholds for considering or rejecting an ECA&D station were adjusted (between 1 and 2 °C). In cases where no SYNOP data were available in an area of ±3° around a target ECA&D station and no comparison was possible in a somewhat larger area of ±4.5°, data were included without any further testing.

In Fig. 1b the distribution of a combined dataset of SYNOP (blue) and ECA&D (red) for T_{avg} in January 2001 is shown. The chosen ECA&D data add valuable information in Scandinavia as well as for Spain and Greece. The total station number is increased here by about 100.

The temporal evolution 2001–2010 of input data for the different parameters is illustrated in Fig. 3. The dotted lines show the fraction of SYNOP reports, the solid lines display the total number of the data used. For wind (grey curve) only SYNOP reports were used, as the number of wind data archived in ECA&D is currently very low. Towards earlier years the availability of SYNOP reports decreases. This decrease is considerable for the Scandinavian region and for many countries around the Mediterranean Sea (compare panels a and b of Fig. 1). ECA&D data contribute especially in

ESSDD
8, 649–702, 2015

these early years. The availablity of SYNOP data is usually higher for T_{min} and T_{max} than for the daily mean values T_{avg} and V_{avg}.

2.3 Quality control and assurance

All input data, the hourly data of each day as well as the daily data of each month, were quality-checked regarding different types of inhomogeneities: (1) outliers, (2) significant shifts in the time series, (3) constant data over longer intervals and (4) exceedance of climatological thresholds. In the following a closer description of the strategies for the example of hourly temperature data is given.

For type (1) the minima and maxima of each daily cycle are substracted from the mean of the cycle while omitting the extremes in the averaging. These test values (denoted dtn and dtx in the program) are considered absolutely (adding notation 1) as well as relatively (divided by the standard deviation of the statistics without extremes, notation 2). Based on experiments with data of several example months empiric thresholds were determined to decide whether a value is considered an outlier or not. Depending on the number of data and the comparison of absolute vs. relative test value these thresholds range between 8–14 °C for $\mathrm{d}tn_1/\mathrm{d}tx_1$ and 4–8 for $\mathrm{d}tn_2/\mathrm{d}tx_2$.

For inconsistencies of types (2) and (3) a running standard deviation (sdr) of five consecutive measurements is calculated. If the minimum of sdr (denoted sdn in the program) reaches zero, at least five identical values in a row are indicated. For a daily series of in total five values (6 hourly data) such an event is highly unlikely and therefore considered a result of erroneous data. In the case of hourly reports the threshold for a rejection is increased to nine identical data in a row. Our sample data showed that certain conditions in winter allow nearly unchanged temperatures over several hours. Also, the change of sdr for each time step is recorded (the maximum difference is denoted $\mathrm{d}sdx$) to identify sudden shifts in the common temperature level. Corresponding tests indicated clear inhomogeneities for dsdx above 7 °C. Climatological thresholds were determined monthly wise for 19 subregions using the full ECA&D archive for 1961–2010. If subregions were insufficiently represented by ECA&D stations, the up-

ESSDD
8, 649–702, 2015

per and lower thresholds were slightly increased and decreased respectively to achieve realistic temperature limits. Additionally, an adjustment of temperature with altitude (assuming 0.65 °C 100 m^{-1}) is carried out to consider stations of high elevation possibly not represented by corresponding data of ECA&D.

For wind data similar strategies, but with adjusted thresholds, were developed to consider erroneous data. Concerning climatological thresholds, a global upper value of 65 m s^{-1} was defined. Here, an approach considering season and region is not helpful, as strong wind events can occur in all regions and throughout the year.

For the time series of daily values similar tests following the strategies for the hourly data are applied. This quality check is particularly important for the extreme values and for the ECA&D data, as related hourly data are often not available. For stations where both extreme values as well as hourly raw data are available, a consistency check between extremes based on these raw data and the time-integrated extremes (denoted raw and int in the following) is made (e.g., minimum T_{min}^{int} is not expected to be above minimum of corresponding hourly data T_{min}^{raw}). For temperature the consistency between the three parameters T_{min}, T_{max} and T_{avg} (e.g., T_{min} expected to be smaller than T_{avg}) is checked for each day, if available.

The hourly data are also used to fill gaps in monthly time series of the extremes, if the overlap between e.g. T_{min}^{int} and T_{min}^{raw} is sufficiently long (more than 10 data points) and the maximum discrepancy between these series is below 2 °C. The estimates from the hourly raw data (e.g., T_{min}^{raw}) are corrected by the mean deviation between both monthly data series to replace missing data of e.g. T_{min}^{int}. Similarly, ECA&D data are used for filling up incomplete monthly SYNOP series if the same coordinates and a high consistency (maximum deviation below 1 °C) are found.

During the interpolation process a monthly background field for each parameter is first created. Therefore, each time series used within one month, must exhibit a nearly complete monthly statistics. Only time series containing less than five missing days within a considered month are used. To achieve a more precise estimate of the monthly mean, the missing values are reconstructed by linear regression with neighbouring

ESSDD
8, 649–702, 2015

stations. If no suitable stations in the neighbourhood are detected and the number of missing data is two or smaller, the mean of the values for the two adjacent dates is used to fill a gap. The values reconstructed in this way are only used to determine the monthly means. For the daily interpolation step missing data are left unchanged, as the interpolation scheme is expected to reproduce missing data more accurate than the rough assumptions used here for the calculation of monthly means.

3 Interpolation procedure temperature

For temperature interpolation, a regression kriging approach (strategy proposed by Ahmed and de Marsily, 1987, and Odeh et al., 1995) adapted from Krähenmann et al. (2011) is used. The interpolation is done in three basic steps: a regression of station monthly means depending on three predictor parameters (elevation, continentality and zonal monthly mean temperatures), followed by interpolation of the regression residuals using kriging to obtain gridded monthly means, and finally, the kriging of daily deviations from station monthly means.

The steps are performed separately in seven overlapping subregions (see Fig. 4; approx. 280 km overlap). The separation roughly follows the climate classification after Köppen and Geiger (e.g. Sanderson, 1999), thus relatively homogeneous conditions for temperature are expected within each region. Compared to Krähenmann et al. (2011) slight modifications were made in the partitioning of the regions in order to adapt them to the MiKlip domain dealt with in this work. By considering subregions instead of the whole domain a better adjustment of the regression model as well as of the kriging parameters (a closer description will follow) during interpolation is achieved. The regional temperature fields of the seven subregions are finally merged by linear weighting in the overlap areas (see Fig. 4).

ESSDD
8, 649–702, 2015

3.1 Regression

In a first step a multiple linear regression of the monthly means for each station against data fields of altitude (using elevation data from the shuttle radar topography mission (SRTM; see http://dds.cr.usgs.gov/srtm/version2_1/SRTM3/), continentality (after Gorczynski, 1920) and zonal monthly mean temperature (climatology 1961–1990 based on CRU TS 3.00; Mitchell and Jones, 2005) is applied (see corresponding fields in Fig. 5).

$$T(x) = k_0 + k_1 \cdot \mathrm{alt}(x) + k_2 \cdot \mathrm{con}(x) + k_3 \cdot \mathrm{zon}(x) + \mathrm{res}(x) \tag{1}$$

with alt: altitude, con: continentality index, zon: zonal mean temperature, res: residuum. These so-called predictor fields explain a major part of the spatial variation of monthly temperatures (Krähenmann et al., 2011). In order to receive a region-specific regression model, usually only data of the core region (weight one, compare Fig. 4) are used to calculate the regression coefficients. Due to the relatively sparse data density in regions 1, 3 and 7, here also data from the overlap areas are considered.

Among the three predictors elevation is the most crucial, as temperature typically strongly depends on it and elevation changes in space occur on very small scales. Thus, linear regression against elevation can substantially improve the final interpolation results in regions with pronounced orographic characteristics. In a new setup applied in this work the dependency of monthly temperature from altitude is determined first and independently from the two other predictors on the basis of station data from mountainous areas. This strategy was chosen, because height coefficients derived from the standard multiple regression are potentially affected by strong horizontal temperature contrasts. Especially for the Scandinavian region implausible lapse rates were diagnosed under such conditions. With an independent regression step on altitude based on data from valleys and mountains in relatively close distance we could solve this issue. The orange dots in Fig. 4 mark stations used for this initial regression step. Depending on the region different criteria (minimum distance to coast, minimum

ESSDD
8, 649–702, 2015

altitude and regional weight) are applied to receive representative subsets. Due to the absence of data suitable for this approach in regions 3 and 7, the regression coefficients for altitude determined in regions 2 and 6 respectively are used here.

A second modification in the altitude regression setup was implemented in this work. Also daily temperature-altitude dependencies are estimated using the same strategy as above. In this way variations from day to day occurring especially in winter can be considered.

For January 2010 we compared the height coefficients according to the previous setup (setup 1, involving all predictors and stations) and the new setup (setup 2, separate regression with subsets). Reference lapse rates were calculated using the regional averages of representative data pairs at the top of mountains and adjacent valleys. A minimum distance of 60 km between adjacent data pairs was chosen to avoid clusters in mountain regions with high station coverage. For region 2 the results from the two setups clearly differ for both, monthly and daily data. Compared to the monthly reference lapse rates a clear overestimation was found for setup 1 (for T_{min} −0.77 vs. −0.11 °C 100 m^{-1} according to reference), while for setup 2 a good agreement was diagnosed (−0.17 vs. −0.11 °C 100 m^{-1} for T_{min}). In comparison with the daily reference lapse rates considerable deviations were found for both setups, with mean absolute deviations of 0.89 and 0.33 °C 100 m^{-1} (T_{min}) for setup 1 (theoretical consideration, since no daily regression implemented in the previous setup) and 2, respectively. However, a clear improvement is achieved with the new setup in this problematic region. For the other regions no significant differences in the results from the two setups occurred in the tested month. In both cases the absolute deviations from the reference lapse rates lie in the range of 0.1 °C 100 m^{-1} or below for monthly and daily data.

Latitudinal changes of the solar radiation as well as land-sea distribution and atmospheric dynamics (preferentially leading to a zonal air mass exchange) affect the predictor parameter of the long-term zonal monthly mean temperature. Continentality reflects the buffering effect of the oceans on annual temperature changes. In contrast to altitude, these two predictor fields exhibit moderate spatial changes. Their potential

ESSDD
8, 649–702, 2015

for improving the interpolation is thus important in regions with a very low observation density, e.g. in North Africa.

Another modification compared to Krähenmann et al. (2011) is the use of station monthly means instead of climatological monthly values as input data for the monthly temperature analysis. In our work monthly hindcast periods are considered instead of current days (as in Krähenmann et al., 2011), therefore the whole monthly statistics are available. By using current monthly means as basis for the linear regression a potentially better adjustment of the regression model to the mean weather conditions observed in this month is achieved and the amplitude of the regression residuals is reduced.

In Table 1 the predictive skills of the three predictors for monthly mean temperature are shown. Listed are the relative explained variances in a regression with single predictors. The corresponding results for the multiple regression model is shown in the last row. All three parameters show a high capacity to predict T_{avg} on a monthly basis. Overall, more than 80 % of the spatial variance can be explained by the three predictors.

3.2 Monthly and daily kriging

The monthly regression residuals (observations minus values according to regression model) are interpolated on a 1.25 km × 1.25 km (0.011°) rotated basic grid (virtual North Pole at 39.25° N, 162° W) using simple kriging. Simple kriging is the least complex kriging algorithm (see e.g. Stahl et al., 2006, for a comparison of the different algorithms). It requires a normal distribution of the data, thus an absence of spatial trends of the mean. This assumption is fulfilled, provided that most of the systematic variance has been removed by the regression step. However, a normal score transformation (following Deutsch and Journel, 1998, attaining a standard normal distribution) is applied to the residuals prior to the interpolation. After interpolation and back transformation block averaging is used to calculate the data on the final target grid of 5 km × 5 km

(0.044°). The sum of regression field and monthly residual field results in the monthly temperature field.

In a third step the differences between daily and monthly temperatures are interpolated following the same concept as above. Before this daily interpolation all daily anomalies are height-corrected using the daily regression coefficients (correcting deviations from monthly mean) for the temperature–altitude relationship determined in step one. The daily temperature field is eventually calculated as the sum of monthly temperatures, daily height-corrected residuals and the reversal of the height correction.

An important aspect in the interpolation using kriging is the adjustment of the kriging parameters (for details see e.g. Deutsch and Journel, 1998). These parameters estimate the change of correlation between nearby stations with distance. The related function considered in kriging is the semivariance γ, describing half the variance between all pairs of data points $Z(x_i)$, $Z(x_j)$ at a certain distance $h = x_i - x_j$ to each other.

$$\gamma(h) = \frac{1}{2N}\sum_{i=1}^{N}\{Z(x_i) - Z(x_j)\}^2 \tag{2}$$

The corresponding graph, illustrated in Fig. 7, is called variogram. The variogram parameters are sill (the maximum semivariance observed in far distance from the origin), nugget (minimum semivariance observed at the origin) and range (the distance at which the semivariance levels off at the maximum). Stations outside the range are not expected to carry relevant information for a target point at the origin. The nugget, taking on values between zero and the sill, defines the noise of the data at the origin. Thus, it sets a basic uncertainty of all final gridded data in the considered region. This nugget effect can be understood as a result of measurement error and fluctuations below the spatial scale resolved by the stations. Different functions can be used to describe the change of the semivariance with distance. Here, a spherical model is assumed, following Krähenmann et al. (2011).

ESSDD
8, 649–702, 2015

Several strategies of fitting the variogram function to the data in each subregion were tested in this work. First, a "null" variogram is defined based on experiments with data from four example months (January 2001, July 2001, January 2010, July 2010). Using cross validation, thus leaving out subsequently one data point and reproducing it based on the information from the remaining stations, different combinations of the three parameters are tested. The parameter values performing best, define the "null" variogram. An automated function for fitting variograms (Pebesma, 2004) is afterwards used to further optimize the variogram. Our tests showed that, on average, both the "null" variogram based on cross validation results and the variogram based on the automated fitting perform equally well, but in rare cases the automated fitting algorithm fails to determine reasonable results due to a missing convergence in the fitting based on least squares (Pebesma, 2004). In the final setup we decided to use the "null" variogram as a robust basis and allow a slight adjustment of the parameters in cases where clear differences between the two models occur. The parameters nugget and range of this "null" variogram are listed in Table 3 for monthly and daily kriging of T_{avg} in the seven subregions. The nugget values can be interpreted as percentage of the background noise measured at the origin. For T_{avg} relatively low nugget-to-sill ratios between 0.1 and 0.3 were determined. Thus, a relatively strong spatial dependence of the residual fields is indicated. The ranges, within which data are correlated with data point at the origin, lie between 5 and 8° on the rotated grid (around 550 to 900 km).

4 Interpolation procedure wind speed

For the interpolation of daily wind speed a new method based on the concept used for temperature was developed. Different predictor fields correlated with wind speed were tested and chosen. Again, the seven subregions displayed in Fig. 4 are applied. In addition, a new subregion for the Alpine region is introduced (Fig. 8). The motivation for this new subregion will be outlined in the next section.

ESSDD

8, 649–702, 2015

4.1 Regression

After testing a variety of potential predictor fields, four parameters were chosen for the linear regression (see Fig. 6).

$$V(x) = k_0 + k_1 \cdot \exp(x) + k_2 \cdot \mathrm{coa}(x) + k_3 \cdot z_0(x) + k_4 \cdot \mathrm{era}(x) + \mathrm{res}(x) \quad (3)$$

with exp: exposure or relative altitude, coa: coastal distance, z_0: surface roughness length, era: ERA-Interim 850 hPa reanalysis wind speed, res: residuum. The use of relative altitude (in the following the term exposure will be used as a synonym) was motivated by Walter et al. (2006), who found good correlations with 10 m wind speed in Germany for altitude at a given point transformed to exposure by dividing it with the mean altitude of the surrounding area of 10 km × 10 km. Here, we calculated corresponding fields on a 1 km grid using elevation data from the shuttle radar topography mission (SRTM; see http://dds.cr.usgs.gov/srtm/version2_1/SRTM3/), applying a radius of 5 km for the determination of surrounding mean altitude. Block averages were calculated to obtain data for the final target grid of 5 km × 5 km. For station data the exact altitude reported is used in comparison with the 1 km grid of mean altitudes described above. We tested different functions to find the most suitable relationship between exposure and 10 m wind speed (e.g. linear, logarithmic and different power functions). On average, exposure to the power of 0.5 turned out to be the best approach.

Coastal distance is also of high relevance for the mean wind speed in 10 m, since the very low roughness across the sea surface, related with very low friction, leads to typically stronger winds in the vicinity of coastlines. Our tests showed the best performance when using the logarithm of the coastal distance in the form ln(coa + 1) and defining maximum coastal distances between 20 and 100 km. This maximum distance is chosen individually for each month and region on the basis of the lowest root mean square error (RMSE) for a regression on coastal distance.

Surface roughness describes the deviations of a surface from an ideal smooth form. On the Earth's surface obstacles such as bushes, trees or buildings increase the surface roughness and thus affect the movement of air. According to theory the wind speed change with distance from the surface shows the following simplified dependency (under stable conditions) on the roughness length z_0 (see e.g. Holton and Hakim, 2012):

$$v(z) = \frac{v_0}{\kappa} \cdot \ln \frac{z}{z_0} \quad (4)$$

with Von Karman constant κ and shear velocity v_0. Based on this equation we apply the roughness length in the regression step as $\ln(10/z_0)$, because linear dependency on v is expected if the variables κ and v_0 are constant. Here, we use roughness length data in 1 km resolution derived from the global land cover dataset GLC2000 (Bartholome and Belward, 2005).

In addition to the three "static" predictor parameters above, the use of meteorological field data can provide valuable information for regions with low station coverage. Krähenmann and Ahrens (2013) showed that the inclusion of remote sensing data from satellite observations as a predictor in regression kriging substantially improves the gridding of surface temperature over the Iberian Peninsula. For wind speed relevant satellite measurements of high quality are currently not available. However, air pressure fields, as the initial driving force of large-scale air movement, are well analysed in weather models. Here, we tested ERA-Interim reanalysis data provided by the European Centre for Medium-Range Weather Forecasts (ECMWF). These data are available in 6 hourly resolution on a reduced Gaussian grid with a grid point distance of approximately 80 km, from 1979 until today (Dee et al., 2011). In order to maintain independence from the other three predictors, corresponding model fields of geopotential height as well as the direct output for wind speed in pressure levels between 850 and 700 hPa (reflecting conditions in the nearly "free" atmosphere, undisturbed by surface impacts) were examined as predictor. Horizontal gradients derived from geopotential height and model wind speeds showed best correlations with surface station wind speed for the lowest tested level 850 hPa.This level corresponds with altitudes of around 1500 m, thus in high mountain areas like the Alpine region the data fields intersect with the land surface, therefore strong horizontal gradients or relatively low model

ESSDD
8, 649–702, 2015

winds respectively occur. In these cases an independence from the predictors exposure and roughness length is not given. In the 700 hPa pressure level the influence of high mountains nearly vanishes but the correlations are generally weaker. For the final regression setup we decided to use ERA-Interim wind fields at 850 hPa. Scalar wind speeds are derived from the two vector components u and v. For grid points above 1000 m reanalysis data are eliminated and afterwards re-estimated by the information of adjacent data points. Finally, daily as well as monthly ERA-Interim scalar wind speed data fields are interpolated to the target Miklip grid using bilinear interpolation.

Despite the filter algorithm applied for reanalysis data in regions of high altitudes a slight dependency of reanalysis data on exposure and roughness length remains for areas like the Alps, the Atlas Mountains, the Caucasus and parts of Turkey. Thus, for the Alps, where a good coverage with station data is available, a new subregion (Fig. 8) was set up, for which regression on reanalysis wind speed is omitted. All grid points above 1500 m in this area receive regional weight one. An overlap to adjacent regions was determined and the regional weights of the adjacent regions were adjusted. Tests indicate a slight improvement of the overall explained variance in three out of four tested months (January/July 2001/2010) for this new configuration.

The four predictors are used for the regression of the monthly mean wind speed data. Core regions relevant for the determination of the regression coefficients in each subregion were defined in the same way as for temperature. For the new region 8 weights above 0.5 define its core area. The test results of the monthly regression for the four example months are listed in Table 2. Each of the parameters explain a considerable part of the spatial variance of V_{avg}. Overall, around 55 % of the variance of the monthly mean is captured by the regression model. The values are somewhat lower than those obtained for temperature regression. This can partly be explained by the high dependency of wind speed on local characteristics not captured by the regression. In contrast to temperature wind speed data tend to produce a logarithmic distribution. Therefore, ratios between monthly wind data and the corresponding area mean of the related region are considered.

ESSDD
8, 649–702, 2015

Also, linear regression on a daily basis was tested, focusing especially on the predictive skill of the daily ERA-Interim reanalysis data. Thereby we found good correlations between ERA-Interim and the daily observations. On average, 31 % of daily variance could be explained by ERA-Interim over four tested months (same as above). Thus, an additional regression step on a daily basis is applied using daily anomalies of ERA-Interim 850 hPa wind data from the corresponding monthly means.

4.2 Monthly and daily kriging

Following the same scheme as described for temperature, the normal-score transformed residuals of the monthly regression are interpolated using simple kriging. Again, a "null" variogram optimized on the basis of cross validation experiments for four tested months (same as above) was determined for monthly and daily means in each region. The results are shown in Table 4. Compared to temperature the nuggets are somewhat larger and the ranges smaller. Thus, for wind speed the noise of the regression residuals at the origin of each target grid point is, on average, relatively large and the interpolation uncertainty relatively high. Regional signals vanish at distances of 2 to 6° (220 to 670 km).

After normal-score back transformation the gridded monthly residuals are added to the gridded regression values and multiplied by the absolute mean wind speed of the considered region (correcting the normalization applied before regression) to obtain the monthly field of V_{avg}.

In the daily kriging step the daily anomalies with respect to the monthly mean at each station are interpolated. Here, ratios instead of absolute deviations are considered, respecting the characteristics of wind speed distribution. As noted in Sect. 4.1, an additional regression with regard to daily ERA-Interim 850 hPa wind speed is performed prior to the interpolation. The final daily wind field is calculated involving the daily regression field, the back transformed daily anomaly ratios and the monthly field of V_{avg}.

5 Uncertainties of interpolation

For each of the three interpolation steps uncertaintiy estimates are recorded. For the two kriging steps the kriging variance is used as a measure of uncertainty. Kriging variance is known to lack precision on a local scale, since local variation of the data is not considered in the estimation of uncertainty. More sophisticated approaches were suggested by Deutsch and Journel (1998) and Yamamoto (2000). However, due to the enormous increase in computing time, as observed in tests using the approach by Yamamoto (2000), we rely on the easily available kriging variance in this work. Regression and kriging errors (kriging variance as well as semivariance at the origin) are combined according to error propagation to determine total uncertainties. Finally, interquartile ranges (IQR, range between 0.25 and 0.75 quantile, thus containg 50 % of the data) are recorded for all monthly and daily gridded datasets.

Furthermore, cross validation for all data within the example years 2001 and 2010 is applied to receive error estimates for all station coordinates. In Sect. 6.4 a comparison between cross validation results and the uncertainty estimates based on kriging variance is presented.

6 Results and discussion

6.1 Example outputs

In Fig. 9 the basic interpolation steps for the generation of the gridded field of daily mean temperature are illustrated. The monthly field (panel c) is calculated as the sum of regression field (a) and the interpolated residuals (b). The interpolated daily anomalies (d) from the monthly data are used to determine the final grid of daily mean temperature (e, here for 31 July 2010). The uncertainties of the daily data are characterized by the IQR fields shown in panel f. In the central and northwestern part of the domain the quality is indicated to be very high, with IQR around 1.0 °C. In other regions, where

ESSDD
8, 649–702, 2015

the coverage of station measurements is lower (compare Fig. 1), higher IQR partly exceeding 3 °C are recorded.

Corresponding results for daily mean wind speed on 28 February 2010 are shown in Fig. 10. Instead of absolute daily anomalies here the ratios to the monthly means are interpolated (panel d). Note that the intermediate step of daily regression on 850 hPa reanalysis winds (as for daily regression on altitude in temperature scheme in Fig. 9) is not displayed here. The uncertainties of the final daily wind speed data are relatively high in areas of high wind speeds. In contrast to temperature, the dependency on the station density is lower, as a considerable amount of the spatial variability is not captured by station measurements and predictor fields (see discussion on the nugget effect in Sect. 4.2). To illustrate the small-scale characteristics of the interpolation products, the two example outputs for daily mean temperature and daily mean wind speed are displayed for Central Europe in Fig. 10a.

6.2 Regression

In the following the results of the monthly regression analysis for the full decade 2001–2010 are presented, for wind speed as well as for the three temperature parameters. In Fig. 11 the spatial variance explained by the predictors (EV) is displayed for the whole decade 2001–2010. Due to a large number of missing data in April 2001 no regression and interpolation results were produced for V_{avg} and T_{avg} in that month. Highest values of up to around 90 % are reached for T_{avg}. For T_{min} and T_{max} the EV fluctuate at slightly lower levels of around 80 %. Concerning wind speed, the EV are considerably lower (around 55 %). Nevertheless, taking into account its high degree of small-scale variability, the EV values realized here for wind speed represent a promising result. Over the 10 years no visible trend as a result of the trend in the number of station data is found. However, the curves indicate annual cycles caused by seasonal changes in spatial variance and/or the predictive capacity of the predictor fields.

This aspect is investigated more closely in Fig. 12. Here, annual cycles based on the statistics over the 10 years for EV as well as the spatial variability (standard deviation)

ESSDD
8, 649–702, 2015

of the raw data and the regression residuals are displayed. For temperature (panels a1, a2; see color code of the three parameters) a generally higher spatial variability during winter is observed. For T_{max} an additional summer maximum is visible, the unexplained variance even peaks in summer for this parameter. However, the high predictive capacity of the three predictors leads to a strong reduction of the residual variability for temperature.

For wind speed (panels b1, b2) similar annual cycles with winter maxima are indicated. After regression the remaining spatial variance is considerably reduced.

6.3 Interpolation – cross validation

For two years, 2001 and 2010, the quality of the interpolation is evaluated by applying cross validation (as defined in Sect. 3.2). Combining the cross validation results for the monthly and the daily interpolation yields uncertainty estimates of the gridded data near each target station. Figure 13 displays corresponding results for January 2010 (panels a1, a2) and July 2010 (b1, b2) for daily mean temperature. Panels a1 and b1 show the mean absolute error of the 31 daily values at each station (see color code). The corresponding statistics over all days and stations are summarized in panels a2 and b2.

The RMSE is 1.68 °C in January and 1.00 °C in July. Thus, interpolation of mean temperature is, on average, considerably more accurate for the summer month considered here. This finding is consistent with the relatively low variability of the regression residuals in summer (compare with Fig. 12). However, the regional distribution of the errors exhibits clear spatial differences: While in the North a tendency towards higher errors in winter is found, the southern regions reveal highest errors mainly in summer. This can possibly be explained by the relatively low predictive capacity for night temperatures during cold winter periods and for day temperatures under hot summer conditions (compare regression residuals in Fig. 12). Especially during periods of temperature inversion in winter the simple linear regression approach on altitude is not capable to reproduce the spatial temperature variation in mountainous regions satis-

ESSDD
8, 649–702, 2015

factorily (e.g. Frei, 2013). A discussion on this aspect will follow in Sect. 8. Overall, very accurate interpolation results are found in regions with a high observation density and low topographic complexity.

Figure 14 shows the results of the cross validation for daily mean wind speed. Again, January (panels a1, a2) and July 2010 (b1, b2) were investigated. As observed for daily mean temperature, also daily mean wind speed shows a somewhat larger spread in the error distribution in January (RMSE of 1.42 compared to 1.06 $\mathrm{m\,s^{-1}}$ in July). However, in the case of wind speed seasonal differences can partly be attributed to the higher mean wind speeds occurring in January 2010 (mean over all stations: 3.37 compared to 3.05 $\mathrm{m\,s^{-1}}$ in July). Relatively high absolute errors are found for stations in coastal and mountainous areas, thus at sites with high wind speeds. Nevertheless, the discrepancies diagnosed for highly exposed stations on the top of mountains typically show a systematic underestimation compared to the observed values (not illustrated in the figure, as absolute deviations are given). Thus, systematic variance caused by the topography is not satisfactorily explained by the regression for areas of very high exposure.

In Fig. 15 the outcomes of cross validation are summarized for the whole annual cycles of 2001 and 2010 for the four parameters: (A) V_{avg}; (B) T_{avg}; (C) T_{min}; and (D) T_{max}. The black and the blue curves illustrate the two cycles of daily RMSE. For comparison the time series of daily standard deviation over all station observations are displayed in brown and orange. In addition to the daily values curves of monthly means are shown. As indicated in Figs. 13 and 14, the interpolation accuracy is clearly higher during warmer seasons for the daily means of wind speed and temperature. Only for T_{max} a tendency towards higher errors in summer is indicated. The interpolation quality is generally somewhat lower for the extreme temperatures (see grey curves for T_{avg} added to the plots C and D for comparison). The temporal averaging used to calculate daily means leads to a reduction of unexplained variance (compare with panel a2 in Fig. 12) und thus increases the accuracy of the interpolation.

ESSDD
8, 649–702, 2015

S. Brinckmann et al.

The variability curves in Fig. 15 can be interpreted as the RMSE for the simple assumption in which the mean over all station data is assigned to each station location. Thus, the difference between lower and upper curves can be understood as a measure for the skill of the interpolation method. For wind speed this skill is much lower than for temperature, due to the large fraction of unexplained variance.

Beside the accuracy of the interpolation, expressed here in the global measure RMSE, also its ability to preserve the observed spatial variability is of importance. Some methods tend to smooth small-scale features (Luo et al., 2008). Regression kriging is known to preserve spatial variance well, provided that the predictors can explain a major part of the observed variance (e.g. Krähenmann et al., 2011). Here, the cross validation results were used to assess this aspect. Figure 16 shows the time series of relative variance, defined here as the ratio of spatial variance of interpolated and observed station data, for the years 2001 and 2010 (see color code indicating the different parameters and years). For the variance of the temperature parameters a good agreement between observations and interpolation results are found. Only for T_{min} significantly underestimated variances are detected during certain periods. For wind speed the relative variances fluctuate around a level slightly below 0.7. This low variance ratio is caused by the high degree of unexplained variance observed on very small scales (nugget effect, Sect. 4.2). The reproduction of the data at a certain station by a weighted average of surrounding data with a large spread leads, on average, to a reduced signal at this station.

6.4 Evaluation of uncertainty estimates

As mentioned in Sect. 5, uncertainty fields based on regression error and kriging variance were determined for each monthly and daily data field. In the following a comparison of these estimates with the findings from cross validation is presented. We use daily cross validation results (as shown in e.g. Fig. 13) and the monthly mean of daily IQR at the nearest adjacent grid points. For each station the number of interpolated data within the IQR error interval is counted for the two example months January and

ESSDD
8, 649–702, 2015

July 2010. The results of this experiment are displayed in Figs. 17 and 18 for daily mean temperature and daily mean wind speed respectively. Blue colors indicate point data for which more daily data lie outside the range of error than expected. Grey dots mark data for which the monthly statistic fairly agrees with the definition of IQR (50 ± 10 %). Points with more accurate data than indicated by the IQR are coloured red. Additionally, corresponding frequency distributions are displayed for the two months (panels a2, b2).

The outcomes for T_{avg} show that IQR uncertainty levels are, on average, relatively consistent with the cross validation results. Nevertheless, small scale changes of the uncertainty, as for e.g. mountainous areas, are not well reflected in the data fields of IQR. In consequence, a tendency towards overestimation of the error in topographically homogeneous regions is observed, while in regions of high topographic complexity errors tend to be underestimated. For July 2010 the distribution is less symmetric than for January 2010. As noted in Sect. 5, local changes of uncertainty as a result of a relatively low or relatively high local variability of the input data are not considered in the kriging variance. This measure mainly depends on the variogram parameters – reflecting average changes of the correlation between adjacent data with distance – and the station density. For certain months the basic variogram parameters determined for each region ("null" variogram, see Sect. 3.2) can deviate significantly from the real data characteristics in that specific month. The restriction of the automated variogram fitting (to avoid instable variogram models, Sect. 3.2), can lead to mean IQR estimates deviating from the mean errors based on cross validation.

For wind speed (Fig. 18) qualitatively similar results are indicated. On average, the IQR defines a reasonable uncertainty range. However, also here the spatial variation is very high. In contrast to temperature, the distribution of significantly outlying data is less systematic for wind speed (a2, b2). This can be explained with its relatively high spatial variability on small scales.

ESSDD
8, 649–702, 2015

7 Summary

In this work interpolation schemes for daily station data of minimum, maximum and mean temperature as well as daily mean wind speed in 5 km resolution for Europe are presented. A regression kriging approach using predictors altitude, continentality and zonal monthly mean temperature, based on the work by Krähenmann et al. (2011), is applied for the temperature parameters. Modifications and further developments were implemented to adapt the existing routine to the special demands of our project. For wind speed a new regression kriging procedure involving the predictor variables exposure, coastal distance, roughness length and 850 hPa ERA-Interim reanalysis wind speeds was developed.

As an important prerequisite for the interpolation, a pre-processing to derive daily means from hourly SYNOP data in combination with a profound quality control was established. Also for the other input data, daily extreme temperatures and the data of the ECA&D archive, detailed quality control procedures were developed. In order to maintain consistency with SYNOP, a selection algorithm, controlling the integration of ECA&D data in regions where SYNOP data are sparse and consistency between the two sources is high, was implemented.

For the time period 2001–2010 the spatial variation of the monthly means can be well explained by the predictors. We obtain relative explained variances in the range of 80–90 % for the temperature parameters and about 50–60 % for wind speed.

Cross validation is performed for the years 2001 and 2010 to assess the quality of the daily interpolation products. For daily mean temperature RMSE of about 1–2 °C are diagnosed. The accuracy for the daily extremes is typically lower, with values around or slightly below 2 °C. In winter interpolation accuracies tend to be reduced compared to summer. For daily maximum temperatures an additional summer reduction in gridding accuracy is detected. The RMSE for daily mean wind speed lies in the range of 1–1.5 $\mathrm{m\,s^{-1}}$. Here, also an annual cycle, with generally smaller errors in summer and higher errors in winter, is indicated.

ESSDD
8, 649–702, 2015

High-resolution daily gridded datasets of air temperature and wind speed for Europe

S. Brinckmann et al.

Concerning the conservation of spatial variance, very good results are found for the temperature parameters. 90–100 % of the observed variance is typically preserved in the interpolation products. Only for minimum temperature at times lower values are recorded. For daily wind speed, a fraction of 60–80 % of the original variance is preserved after interpolation. The relatively high degree of unexplained small-scale variance leads to a smoothing of the wind data.

The cross validation results are also used to evaluate the quality of the gridding uncertainty based on kriging variance and regression errors. On average, a reasonable consistency between these data is found. Nevertheless, temporal and spatial variations of uncertainty occurring on small scales are not adequately reflected in the gridded uncertainties.

8 Conclusions

The regression kriging approaches used in this work for the interpolation of daily temperature and wind speed observations on a grid size of 0.044° (5 km) show good performance in terms of accuracy and variance preservation. With the inclusion of suitable predictor variables small-scale characteristics of the meteorological parameters can be well captured.

For the dependency of temperature on altitude more reliable regression results are obtained by performing this regression separately and on the basis of representative stations. Also, day-to-day variations of this dependency are considered in the new setup used in this study. Nevertheless, the linear regression approach applied to the relatively large areas of each subregion is not capable to reflect non-linear vertical temperature changes and spatial differences of this parameter within a subregion. More complex approaches considering this issue in the calculation of high-resolution gridded data in mountainous reagions have been published (e.g. Frei, 2013). However, these specialized strategies require the presence of stations representative for a certain area and altitude level. For the relatively large domain dealt with in our work, where

ESSDD
8, 649–702, 2015
High-resolution daily gridded datasets of air temperature and wind speed for Europe
S. Brinckmann et al.

many mountain regions are insufficiently represented by station data, the inclusion of reanalysis data describing the vertical temperature structure might offer a promising strategy in this respect.

Concerning the regression of wind speed, a considerable part of spatial variance on a monthly basis (40–50 %) remains unexplained by the predictors used in this work. For predictors exposure, coastal distance and roughness length it would be more realistic to take into account the current wind direction and local predictor conditions determined for this wind direction. This strategy would introduce further complexity in the calculations. On the other hand the percentage of variance explained by predictors as well as the final interpolation accuracy could likely be increased.

The gridded error estimates calculated for the daily and monthly products are, on regional average, reasonable but for certain days and areas these estimates are found to be unrealistic. An alternative approach yielding more reliable errors (Yamamoto, 2000) was not implemented due to the enormous increase in computing time. Thus, the determination of accurate uncertainty estimates remains an issue for datasets of high resolution in space and time.

Acknowledgements. The authors would like to acknowledge the Bundesministerium für Bildung und Forschung (BMBF) for funding this project. The colleagues in the department Regional Climate Monitoring at Deutscher Wetterdienst (DWD) are acknowledged, especially Maya Körber and Andrea Kreis for their support in technical issues related with UNIX and database queries. We also thank our partners participating in the DecReg project for the fruitful cooperation during the 26 months. Furthermore, the data providers in the ECA&D project are acknowledged (Klein Tank et al., 2002).

References

Ahmed, S. and de Marsily, G.: Comparison of geostatistical methods for estimating transmissivity using data on transmissivity and specific capacity, Water Resour. Res., 23, 1717–1737, doi:10.1029/WR023i009p01717, 1987. 658

Bartholome, E. and Belward, A. S.: GLC2000: a new approach to global land cover mapping from Earth observation data, Int. J. Remote Sens., 26, 1959–1977, doi:10.1080/01431160412331291297, 2005. 665

Dee, D. P., Uppala, S. M., and Simmons, A. J. E. A.: The ERA-Interim reanalysis: configuration and performance of the data assimilation system, Q. J. Roy. Meteor. Soc., 137, 553–597, doi:10.1002/qj.828, 2011. 665

Deutsch, C. V. and Journel, A.: GSLIB: Geostatistical Software Library and User's Guide, 2nd edn., Oxford University Press, New York, 1998. 661, 662, 668, 690

Frei, C.: Interpolation of temperature in a mountainous region using nonlinear profiles and non-Euclidean distances, Int. J. Climatol., 34, 1585–1605, doi:10.1002/joc.3786, 2013. 671, 675

Gerth, W.-P. and Christoffer, J.: Windkarten von Deutschland, Meteorol. Z., 3, 67–77, 1994. 652

Gorczynski, L.: Sur le calcul du degré de continentalisme et son application dans la climatologie, Geografiska Annaler, 2, 324–331, 1920. 659

Hansen, J., Ruedy, R., Sato, M., and Lo, K.: Global surface temperature change, Rev. Geophys., 48, RG4004, doi:10.1029/2010RG000345, 2010. 651

Haylock, M. R., Hoftsra, N., Klein Tank, A. M. G., Klok, E. J., Jones, P. D., and New, M.: A European daily high-resolution gridded data set of surface temperature and precipitation for 1950–2006, J. Geophys. Res., 113, D20119, doi:10.1029/2008JD010201, 2008. 651

Hogewind, F. and Bissolli, P.: Operational maps of monthly mean temperature for WMO Region VI (Europe and Middle East), Idojaras, 115, 31–49, 2011. 651

Holton, J. R. and Hakim, G. J.: An Introduction to Dynamic Meteorology, 5th edn., Academic Press, Waltham, MA, USA, 2012. 665

Klein Tank, A. M. G., Wijngaard, J. B., Können, G. P., Böhm, R., Demarée, G., Gocheva, A., Mileta, M., Pashiardis, S., Hejkrlik, L., Kern-Hansen, C., Heino, R., Bessemoulin, P., Müller-Westermeier, G., Tzanakou, M., Szalai, S., Pálsdóttir, T., Fitzgerald, D., Rubin, S., Capaldo, M., Maugeri, M., Leitass, A., Bukantis, A., Aberfeld, R., van Engelen, A. F. V., Forland, E., Mietus, M., Coelho, F., Mares, C., Razuvaev, V., Nieplova, E., Cegnar, T., Antonio López, J., Dahlström, B., Moberg, A., Kirchhofer, W., Ceylan, A., Pachaliuk, O., Alexander, L. V., and Petrovic, P.: Daily dataset of 20th-century surface air temperature and precipitation series for the European Climate Assessment, Int. J. Climatol., 22, 1441–1453, doi:10.1002/joc.773, 2002. 653, 676

Discussion Paper | Discussion Paper | Discussion Paper | Discussion Paper |

ESSDD

8, 649–702, 2015

High-resolution daily gridded datasets of air temperature and wind speed for Europe

S. Brinckmann et al.

Krähenmann, S. and Ahrens, B.: Spatial gridding of daily maximum and minimum 2-m temperatures supported by satellite observations, Meteorol. Atmos. Phys., 120, 87–105, doi:10.1007/s00703-013-0237-9, 2013. 665

Krähenmann, S., Bissolli, P., Rapp, J., and Ahrens, B.: Spatial gridding of daily maximum and minimum temperatures in Europe, Meteorol. Atmos. Phys., 114, 151–161, doi:10.1007/s00703-011-0160-x, 2011. 650, 658, 659, 661, 662, 672, 674

Li, J. and Heap, A. D.: A review on spatial interpolation methods for environmental scientists, Geoscience Australia, 15, doi:10.1127/0941-2948/2006/0162, 2008. 652

Luo, W., Taylor, C., and Parker, S. R.: A comparison of spatial interpolation methods to estimate continuous wind speed surfaces using irregularly distributed data from England and Wales, Int. J. Climatol., 28, 947–959, doi:10.1002/joc.1583, 2008. 652, 672

Matheron, G.: Principles of geostatistics, Econ. Geol., 58, 1246–1266, 1963. 653

Mitchell, T. D. and Jones, P. D.: An improved method of constructing a database of monthly climate observations and associated highresolution grids, Int. J. Climatol., 25, 693–712, doi:10.1002/joc.1181, 2005. 659

Morice, C. P., Kennedy, J. J., Rayner, N. A., and Jones, P. D.: Quantifying uncertainties in global and regional temperature change using an ensemble of observational estimates: the HadCRUT4 data set, J. Geophys. Res., 117, D08101, doi:10.1029/2011JD017187, 2012. 651

Odeh, I. O. A., McBratney, A. B., and Chittleborough, D. J.: Further results on prediction of soil properties from terrain attributes: heterotropic cokriging and regression-kriging, Geoderma, 67, 215–226, doi:10.1016/0016-7061(95)00007-B, 1995. 658

Pebesma, E. J.: Multivariable geostatistics in S: the gstat package, Comput. Geosci., 30, 683–691, doi:10.1016/j.cageo.2004.03.012, 2004. 663

Rohde, R., Muller, R., Jacobsen, R., Perlmutter, S., Rosenfeld, A., Wurtele, J., Curry, J., Wickham, C., and Mosher, S.: Berkeley Earth Temperature Averaging Process, Geoinfor. Geostat.: An Overview 1:2. doi:10.4172/2327-4581.1000103, 2013. 651

Sanderson, M.: The classification of climates from Pythagoras to Koeppen, B. Am. Meteorol. Soc., 80, 669–673, doi:10.1175/1520-0477(1999)080<0669:TCOCFP>2.0.CO;2, 1999. 658

Smith, T. M., Reynolds, R. W., Peterson, T. C., and Lawrimore, J.: Improvements to NOAA's historical merged land–ocean surface temperature analysis (1880–2006), J. Climate, 21, 2283–2296, doi:10.1175/2007JCLI2100.1, 2008. 651

Stahl, K., Moore, R. D., Floyer, J. A., Asplin, M. G., and McKendry, I. G.: Comparison of approaches for spatial interpolation of daily temperature in a large region with complex topography and highly variable station density, Agr. Forest Meteorol., 139, 224–236, doi:10.1016/j.agrformet.2006.07.004, 2006. 661

van den Besselaar, E. J. M., Klein Tank, A. M. G., van der Schrier, G., and Jones, P. D.: Synoptic messages to extend climate data records, J. Geophys. Res., 117, D07101, doi:10.1029/2011JD016687, 2012. 655

Walter, A., Keuler, K., Jacob, D., Knoche, R., Block, A., Kotlarski, S., Müller-Westermeier, G., Rechid, D., and Ahrens, W.: A high resolution reference data set of German wind velocity 1951–2001 and comparison with regional climate model results, Meteorol. Z., 2008/23, 585–596, 2006. 652, 664

Yamamoto, J. K.: An alternative measure of the reliability of ordinary kriging estimates, Math. Geol., 32, 489–509, doi:10.1023/A:1007577916868, 2000. 668, 676

ESSDD

8, 649–702, 2015

Title Page

Abstract | Instruments

Data Provenance & Structure

Tables | Figures

Back | Close

Full Screen / Esc

Printer-friendly Version

Interactive Discussion

Table 1. Whole-domain averages of spatial variance explained by single predictors [%] for monthly mean temperature and four tested months. In the bottom row the results for the multiple regression model involving all predictors are given.

Predictor	Jan 2001	Jan 2010	Jul 2001	Jul 2010
Altitude	40	23	38	41
Continentality	28	33	52	53
Zonal mean temperature	30	37	41	25
All	85	84	84	83

ESSDD
8, 649–702, 2015

Table 2. Whole-domain averages of the spatial variance explained by single predictors [%] for monthly mean wind speed and four tested months. The bottom row shows the result for the multiple regression model involving all predictors.

Predictor	Jan 2001	Jan 2010	Jul 2001	Jul 2010
Exposure	24	20	18	17
Coastal distance	28	35	27	28
Roughness length	23	28	22	24
ERA-Interim 850 hPa	10	13	11	21
All	58	58	51	53

ESSDD
8, 649–702, 2015

Table 3. Regional variogram parameters nugget (relative to sill) and range [° rot. grid] based on experiments with temperature data T_{avg} of four example months January 2001, July 2001, January 2010 and July 2010. Listed are the regional averages for monthly and daily interpolation.

Parameter	Region 1	Region 2	Region 3	Region 4	Region 5	Region 6	Region 7
Monthly							
Nugget	0.1	0.1	0.1	0.1	0.1	0.2	0.1
Range	5	5	7	6	8	6	7
Daily							
Nugget	0.3	0.1	0.1	0.2	0.1	0.2	0.1
Range	6	6	8	6	8	7	8

ESSDD

8, 649–702, 2015

High-resolution daily gridded datasets of air temperature and wind speed for Europe

S. Brinckmann et al.

Table 4. Regional variogram parameters nugget (relative to sill) and range [° rot.grid] based on experiments with wind speed data V_{avg} of four example months (January 2001, July 2001, January 2010 and July 2010). Listed are the regional averages for monthly and daily interpolation.

Parameter	Region 1	Region 2	Region 3	Region 4	Region 5	Region 6	Region 7	Region 8
Monthly								
Nugget	0.6	0.7	0.1	0.5	0.6	0.6	0.8	0.2
Range	8	3	7	5	5	5	2	3
Daily								
Nugget	0.7	0.4	0.5	0.3	0.4	0.4	0.5	0.7
Range	2	4	5	3	4	3	4	1

ESSDD
8, 649–702, 2015

High-resolution daily gridded datasets of air temperature and wind speed for Europe

S. Brinckmann et al.

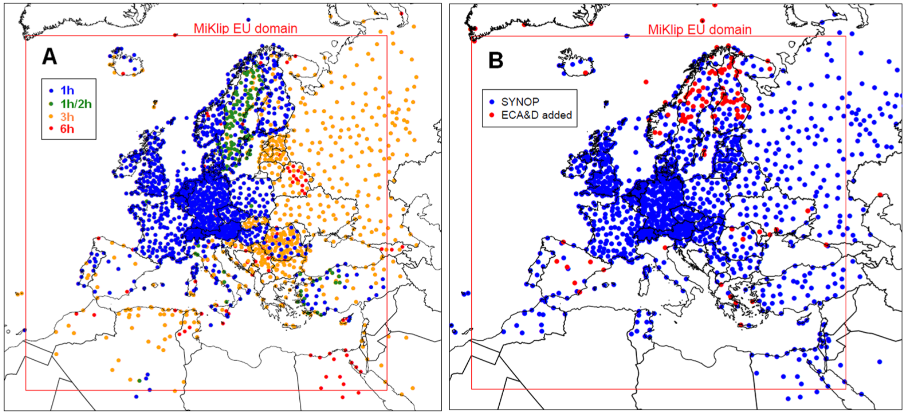

Figure 1. (a) SYNOP stations with hourly data in target MiKlip EU domain for January 2010. The color code indicates the frequency of reports (between 1 and 6 h). The station records marked green contain hourly data but show gaps for the main dates 00:00, 03:00, 06:00 UTC, etc. **(b)** SYNOP data for T_{avg} (blue) in January 2001 and added ECA&D data using selection algorithm described in the text.

ESSDD
8, 649–702, 2015

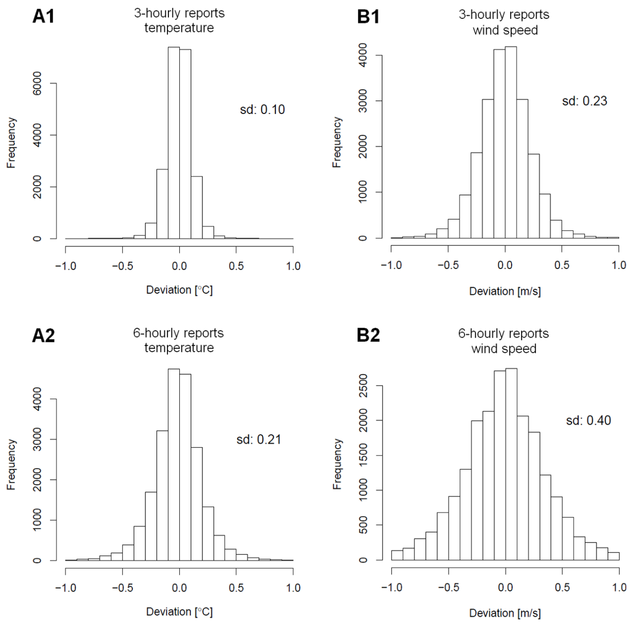

Figure 2. Accuracy of daily mean temperatures **(a1, a2)** and daily mean wind speeds **(b1, b2)** in January 2001 for different frequencies of observation (3 and 6 h) using 1 hourly data as reference. The standard deviations, denoted sd, are added to the histograms.

ESSDD
8, 649–702, 2015

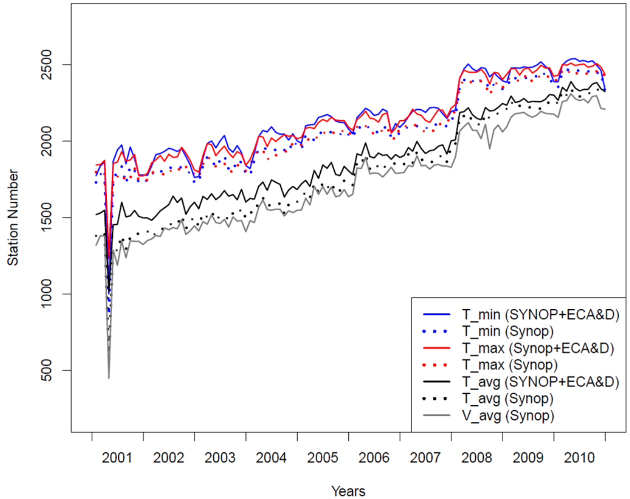

Figure 3. Temporal evolution of total input data used for the interpolations 2001–2010 (see color code). The dotted curves show the basic number made up by SYNOP stations. The differences indicate the increase by the inclusion of ECA&D data. For wind speed only SYNOP data are used for the interpolations.

ESSDD
8, 649–702, 2015

High-resolution daily gridded datasets of air temperature and wind speed for Europe

S. Brinckmann et al.

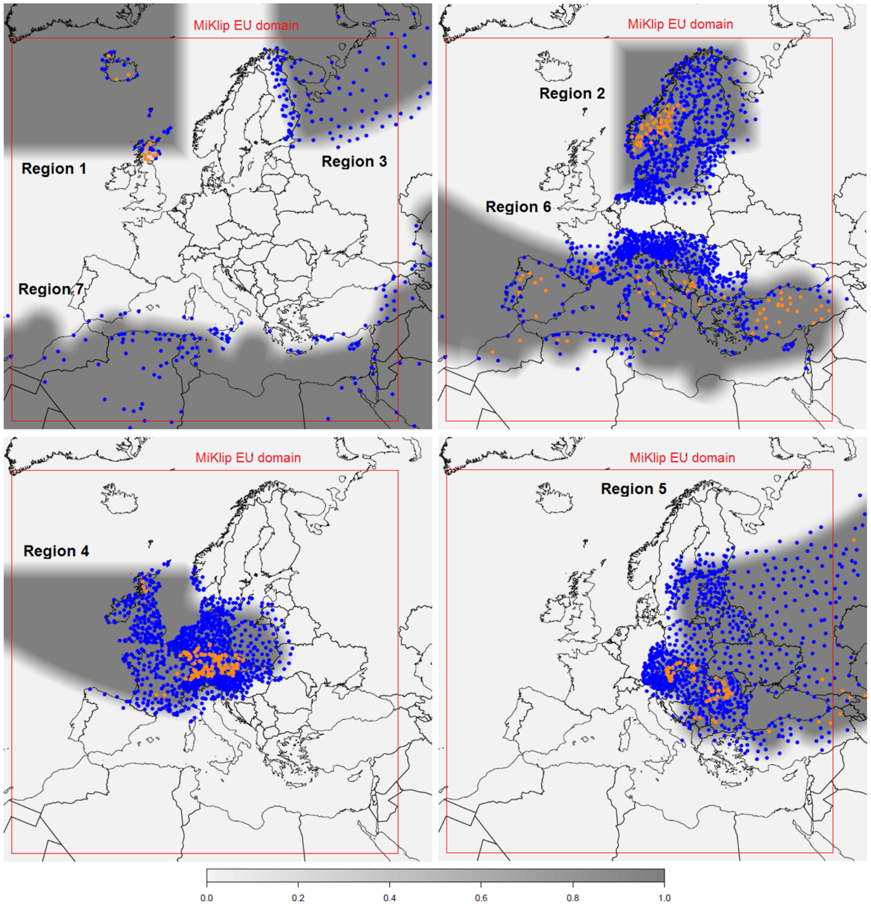

Figure 4. The seven subregions used for temperature interpolation. The regional fields are finally merged using the regional weights (grey color scale). Stations used to calculate regional lapse rates are orange.

ESSDD
8, 649–702, 2015

High-resolution daily gridded datasets of air temperature and wind speed for Europe

S. Brinckmann et al.

Title Page
Abstract
Instruments
Data Provenance & Structure
Tables
Figures
Back
Close
Full Screen / Esc
Printer-friendly Version
Interactive Discussion

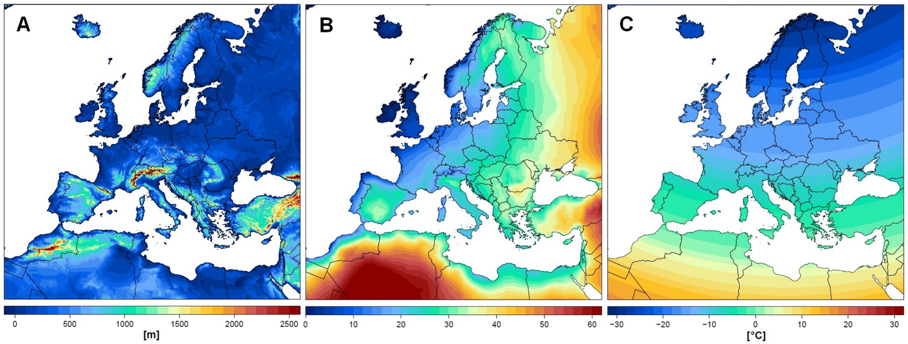

Figure 5. Predictor fields of altitude **(a)**, continentality **(b)** and zonal monthly mean temperature (**c**; here January, based on climatology 1961–1990).

ESSDD
8, 649–702, 2015

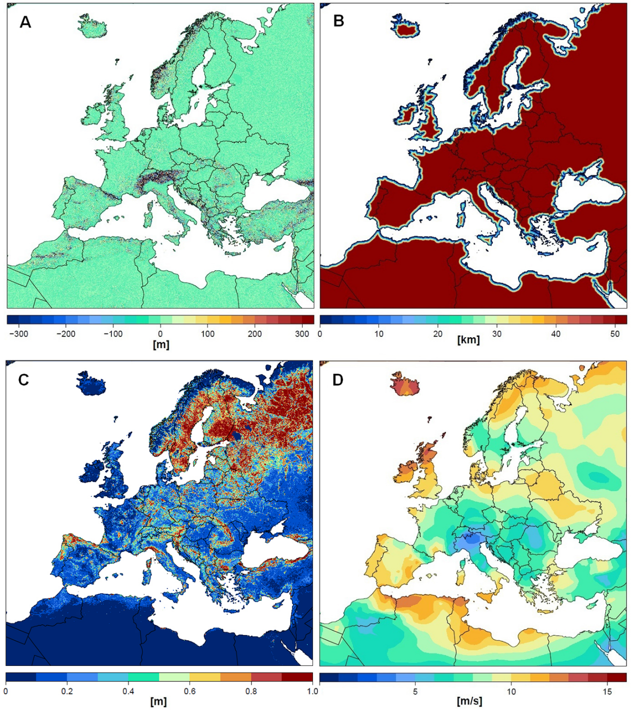

Figure 6. Predictor fields of exposure **(a)**, coastal distance **(b)**, roughness length **(c)**, ERA-Interim mean scalar wind velocity in 850 hPa (**d**; here January 2001).

ESSDD
8, 649–702, 2015

High-resolution daily gridded datasets of air temperature and wind speed for Europe

S. Brinckmann et al.

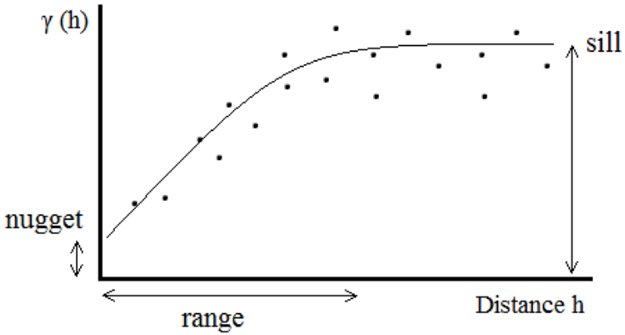

Figure 7. Variogram with the parameters nugget, sill and range (after Deutsch and Journel, 1998). See description in the text.

ESSDD
8, 649–702, 2015

High-resolution daily gridded datasets of air temperature and wind speed for Europe

S. Brinckmann et al.

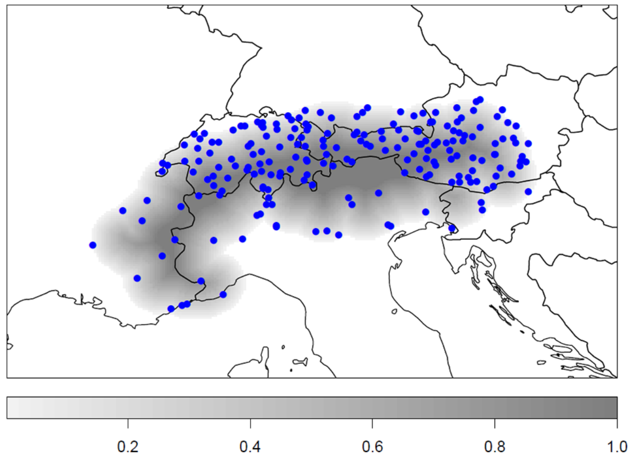

Figure 8. Alpine subregion (denoted region 8 in the following) introduced for the interpolation of wind speed.

ESSDD
8, 649–702, 2015

High-resolution daily gridded datasets of air temperature and wind speed for Europe

S. Brinckmann et al.

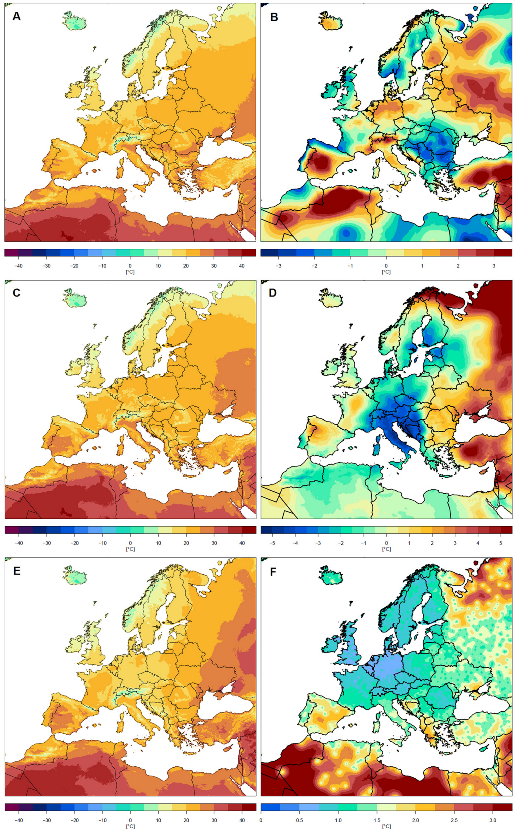

Figure 9. Steps in the interpolation of daily mean temperature for 31 July 2010. **(a)** Monthly regression field; **(b)** monthly regression residuals; **(c)** monthly mean temperature; **(d)** daily anomaly with respect to monthly mean temperature; **(e)** daily mean temperature; **(f)** interquartile range of daily mean temperature.

ESSDD

8, 649–702, 2015

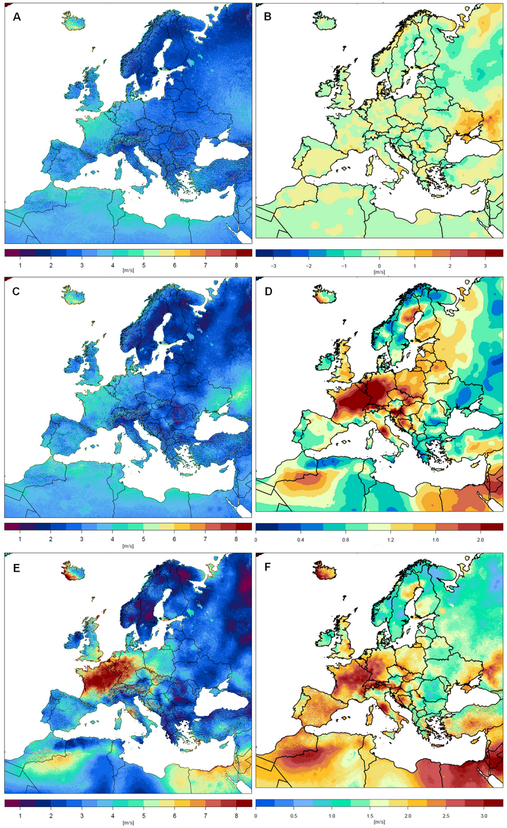

Figure 10. Steps in the interpolation of daily mean wind speed for 28 February 2010. **(a)** Monthly regression field; **(b)** monthly regression residuals; **(c)** monthly mean wind speed; **(d)** ratio daily to monthly mean wind speed; **(e)** daily mean wind speed; **(f)** interquartile range of daily mean wind speed.

ESSDD
8, 649–702, 2015

High-resolution daily gridded datasets of air temperature and wind speed for Europe

S. Brinckmann et al.

Title Page
Abstract | Instruments
Data Provenance & Structure
Tables | Figures
◀| |▶
◀ ▶
Back | Close
Full Screen / Esc
Printer-friendly Version
Interactive Discussion

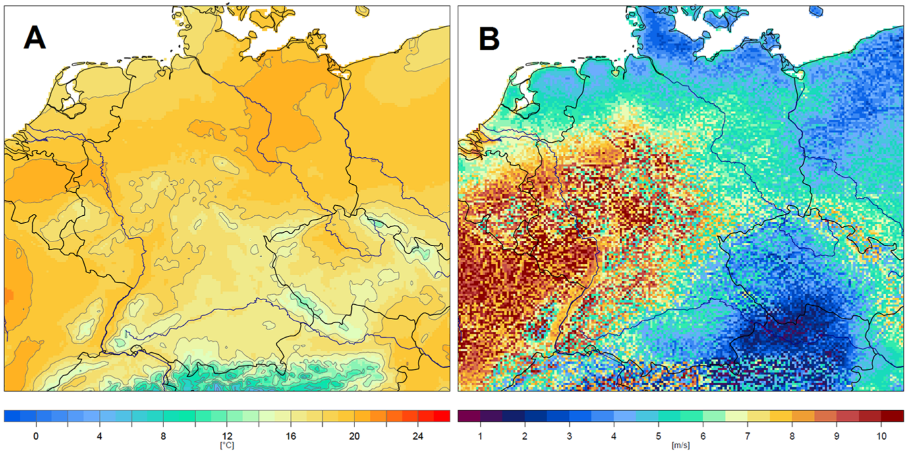

Figure 11. Detailed image of Central Europe for **(a)** daily mean temperature (31 July 2010) and **(b)** daily mean wind speed (28 February 2010).

ESSDD
8, 649–702, 2015

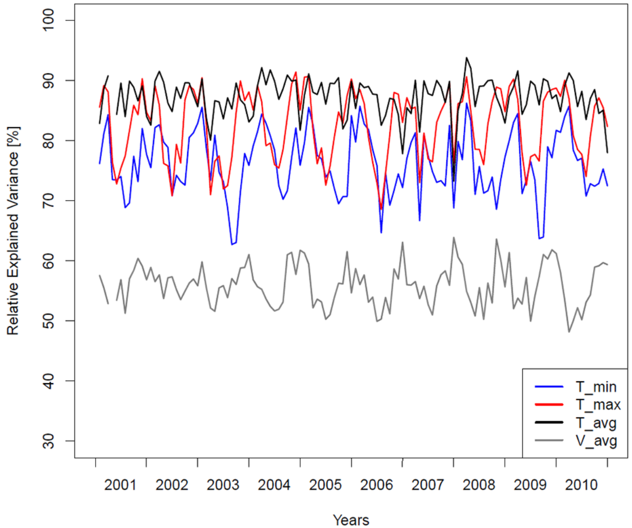

Figure 12. Relative explained variance for monthly mean wind speed and for the monthly mean of the three temperature parameters (see color code) for 2001–2010.

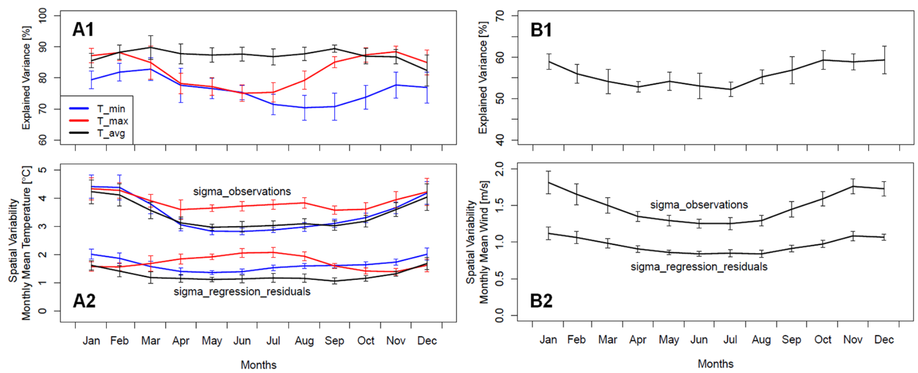

Figure 13. Annual cycles (means 2001–2010) of relative explained variance for monthly mean temperature (**a1**, see color code of the parameters) and wind speed **(b1)** and corresponding spatial variability (1σ) before and after regression **(a2, b2)**. All data are given as means over all subregions. The error bars display the temporal standard deviation over the 10 years.

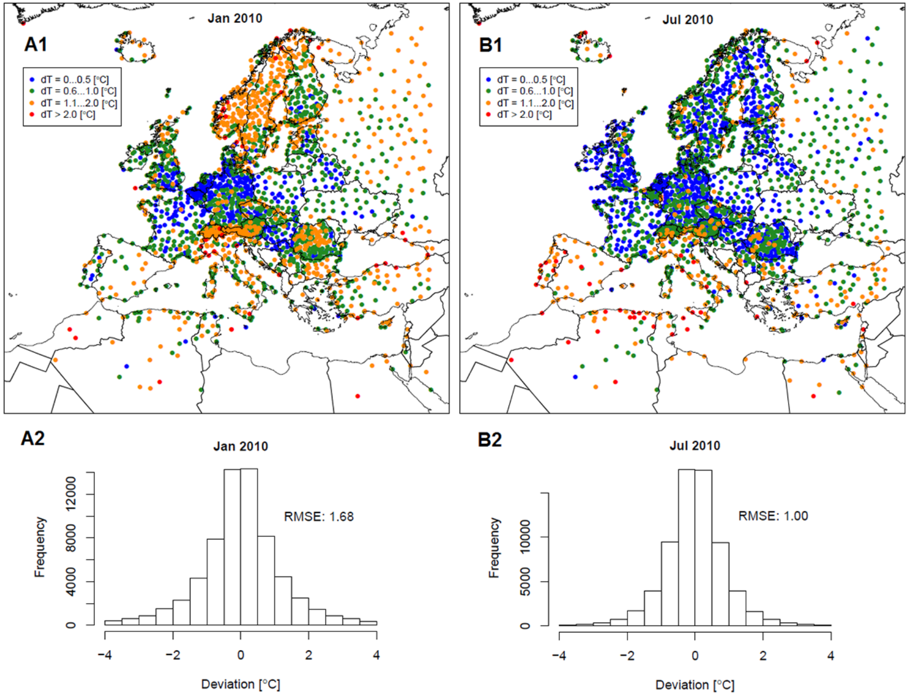

Figure 14. Cross validation results for daily mean temperature data January 2010 **(a1, a2)** and July 2010 **(b1, b2)**. The color code indicates the monthly mean of the daily absolute deviations. The histograms contain the full statistics of deviations over all days and stations.

ESSDD
8, 649–702, 2015

High-resolution daily gridded datasets of air temperature and wind speed for Europe

S. Brinckmann et al.

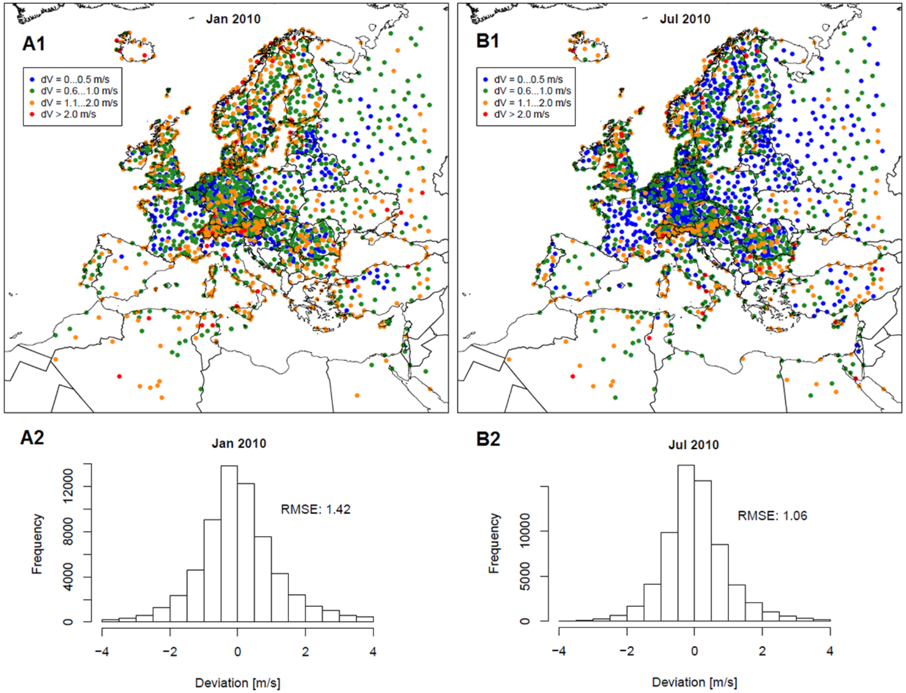

Figure 15. Cross validation results for daily mean wind speed data January 2010 **(a1, a2)** and July 2010 **(b1, b2)**. The color code indicates the monthly mean of the daily absolute deviations. The histograms contain the full statistics of deviations over all days and stations.

ESSDD
8, 649–702, 2015

High-resolution daily gridded datasets of air temperature and wind speed for Europe

S. Brinckmann et al.

Title Page
Abstract | Instruments
Data Provenance & Structure
Tables | Figures
◄◄ | ►►
◄ | ►
Back | Close
Full Screen / Esc
Printer-friendly Version
Interactive Discussion

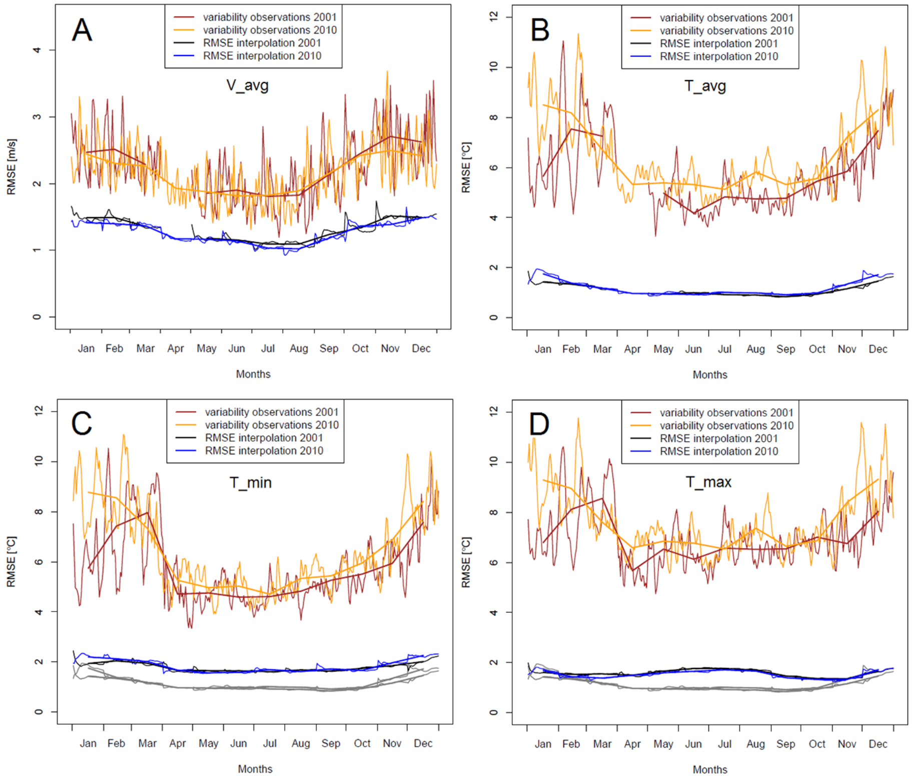

Figure 16. Annual cycle of daily RMSE according to cross validation for 2001 (black) and 2010 (blue) for: **(a)** mean wind speed V_{avg}; **(b)** mean temperature T_{avg}; **(c)** minimum temperature T_{min}; and **(d)** maximum temperature T_{max}. For comparison the daily standard deviation over all station observations is displayed in brown (2001) and orange color (2010). To all data corresponding curves of monthly means are added. In panels **(c)** and **(d)** the RMSE data for T_{avg} are displayed in grey color for comparison.

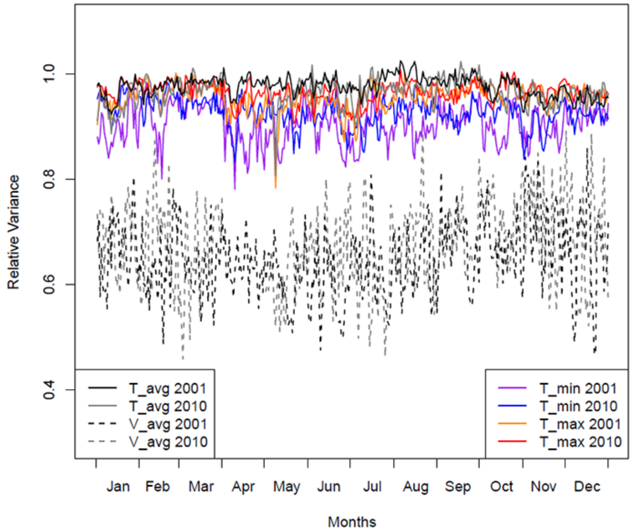

Figure 17. Time series of the ratio of spatial variance of interpolated vs. observed station data for the years 2001 and 2010 based on cross validation. The color code indicates the parameters and years.

ESSDD
8, 649–702, 2015

High-resolution daily gridded datasets of air temperature and wind speed for Europe

S. Brinckmann et al.

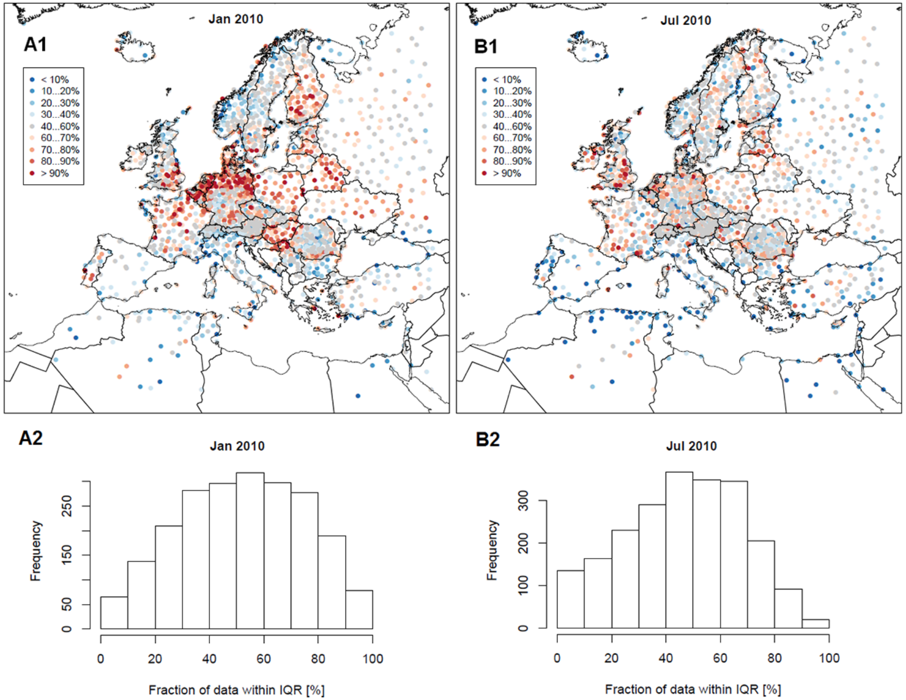

Figure 18. Comparison of cross validation results with gridded uncertainty estimates for daily mean temperature in January 2010 **(a1)** and July 2010 **(b1)**: Fraction of interpolated daily data at stations within nearest neighbour gridded IQR (interquartile range). Blue colors indicate an underestimation, red colors an overestimation of the uncertainty. In panels **(a2)** and **(b2)** corresponding frequency distributions are displayed.

ESSDD
8, 649–702, 2015

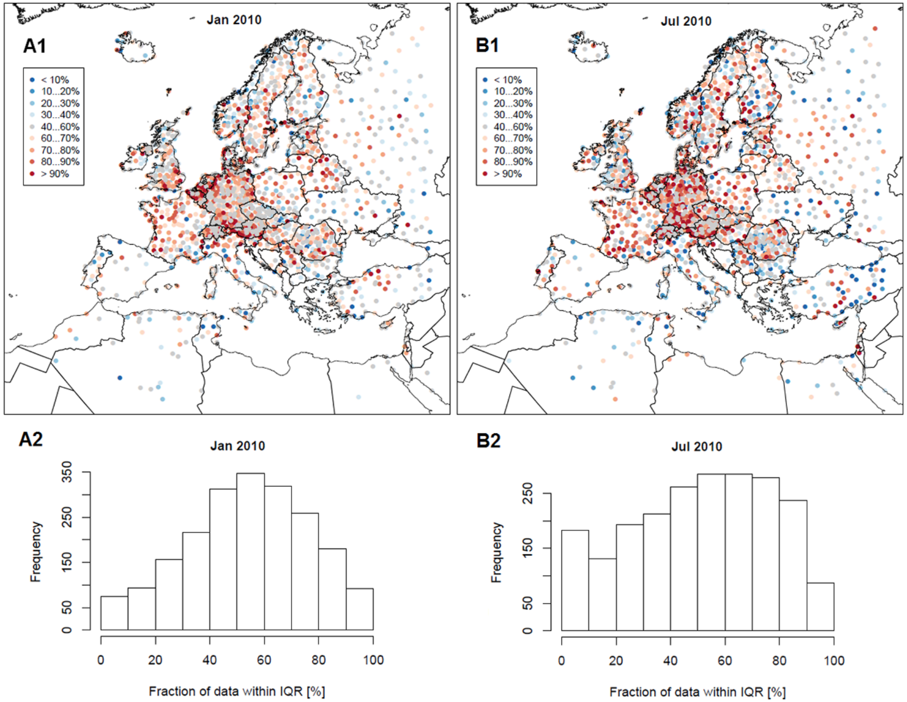

Figure 19. Comparison of cross validation results with gridded uncertainty estimates for daily mean wind speed in January 2010 **(a1)** and July 2010 **(b1)**: Fraction of interpolated daily data at stations within nearest neighbour gridded IQR (interquartile range). Blue colors indicate an underestimation, red colors an overestimation of the uncertainty. In panels **(a2)** and **(b2)** corresponding frequency distributions are displayed.

ESSDD
8, 649–702, 2015